Catalysis Science & Technology

ROYAL SOCIETY OF CHEMISTRY

PAPER

View Article Online
View Journal



Cite this: DOI: 10.1039/d0cy00183j

# Aerobic oxidation of 1,6-hexanediol to adipic acid over Au-based catalysts: the role of basic supports

Noemi Capece,[ab] Achraf Sadier,[a] Camila Palombo Ferraz,[a] Joëlle Thuriot-Roukos,[a] Mariusz Pietrowski,[c] Michał Zieliński,[c] Sébastien Paul,[a] Fabrizio Cavani[b] and Robert Wojcieszak*[a]

Received 29th January 2020,
Accepted 28th March 2020

DOI: 10.1039/d0cy00183j

rsc.li/catalysis

1,6-Hexanediol is one of the most relevant building blocks originating from biomass and it transforms into adipic acid for polymer synthesis. Herein, we examine the selective oxidation of 1,6-hexanediol to adipic acid over Au-based catalysts, in the aqueous phase, under base-free conditions. Particularly, the absence of a base allows the neutralization step at the end of the reaction to be avoided. The influences of various supports (MgO, BaO, NiO, and $TiO_2$) and substrate/gold molar ratios were studied. Under the conditions used, the leaching of Mg in the mixture of $MgF_2$ and MgO was limited by diluting the basic sites in the support. The highest selectivity to adipic acid (43%) was achieved at 110 °C under 15 bar of air in the presence of 2 wt% Au/0.6$MgF_2$–0.4MgO.



## Introduction

Adipic acid (AA) is an important aliphatic dicarboxylic acid with the highest world production and is mostly used as a starting material in the synthesis of polyamide (nylon-6,6), fibers, adipic esters as plasticizers in PVC, polyurethanes, lubricants, food additives and many other applications.[1,2] In 2014, 2839 kton was the global production and it is predicted to further grow with about 2% increase each year.[3] It is due also to the retreat of the nylon sector over non-nylon applications.[4] AA is generally synthesized by a two-step oxidation process. In the first step, the oxidation of cyclohexane to a mixture of cyclohexanone/cyclohexanol (one/Ol, KA oil) is performed in air and in the second step the oxidation of KA oil to AA with an excess of nitric acid $HNO_3$, which is seriously harmful to the environment leading to a huge impact on global warming. Indeed, the nitrous oxide ($N_2O$) produced in this process is an unavoidable stoichiometric waste that is commonly considered as a major contributor to global warming and ozone depletion.[5] Moreover, AA can be obtained *via* catalytic petrochemical routes including the oxidation of cyclohexane with molecular $O_2$,[6,7] of cyclohexanol/one with air[8] or hydrogen peroxide,[9] of cyclohexene with hydrogen peroxide,[10,11] and of *n*-hexane,[12] or through methoxycarbonylation of 1,3-butadiene followed by hydrolysis.[13] On the other hand, the bio-based production of AA has become an alternative candidate to the petrochemical process.[3,14,15] In an alternative approach, Boussie *et al.*[16] presented a two-step catalytic process for the synthesis of AA. 99% yield of AA was obtained by C–O bond hydrogenolysis of tetrahydrofuran-2,5-dicarboxylic acid (obtained by the hydrogenation of 2,5-furandicarboxylic acid, yield of 88%).[16] In parallel, Boussie *et al.*[17,18] discovered a new heterogeneous catalyst to produce AA in two steps from glucose: first, 66% of glucaric acid was obtained by oxidation of an aqueous solution of glucose in the presence of a Pt/$SiO_2$ catalyst, followed by selective catalytic hydrodeoxygenation of glucaric acid to AA (89% yield) over a PdRh/$SiO_2$ catalyst and a halogen source. Another route is a two-step reaction starting with the acid catalyzed ring opening of γ-valerolactone to pentenoic acid in the presence of a silica/alumina catalyst, and its subsequent conversion to AA on a palladium acetate catalyst in the presence of CO and water.[19] Recently, scientific attention has been paid toward another bio-based route to produce AA by the oxidation of bio-HDO and oxidative cleavage of *trans*-1,2-cyclohexanediol.[20] The synthesis of bio-HDO from renewable feedstocks has been disclosed using many catalytic reaction pathways: i) selective C–O bond hydrogenolysis of 2,5-tetrahydrofurandimethanol,[21,22] ii) selective ring opening of the intermediate tetrahydropyran-2-methanol,[21,23,24] or its sequential dehydration/hydration/hydrogenation,[25] iii) hydrogenolysis of sorbitol,[26,27] and (iv) hydrogenation of levoglucosenone.[28] However, the HDO yield was still moderate (25–40%). The biological oxidation of HDO to AA was previously reported.[29] Nevertheless, the catalytic

[a] *Univ. Lille, CNRS, Centrale Lille, ENSCL, Univ. Artois UMR 8181 – UCCS – Unité de Catalyse et Chimie du Solide, F-59000 Lille, France.*
*E-mail: Robert.wojcieszak@univ-lille.fr*
[b] *Dipartimento di Chimica Industriale "Toso Montanari", Università di Bologna, Viale Risorgimento 4, 40136 Bologna, Italy*
[c] *Faculty of Chemistry, Adam Mickiewicz University in Poznań, Uniwersytetu Poznańskiego 8, 61-614 Poznań, Poland*

oxidation of aldehydes or alcohols over a noble metal based catalyst in the presence of molecular oxygen is also probable.[30–33] A 2.69 wt% Pt/C catalyst yielded 85% AA in 0.35 M acetic acid at 100% conversion after 24 h of reaction at 70 °C under 10 bar $O_2$, using a molar substrate/metal ratio of 100.[31] On the other hand, the oxidation of an aqueous solution of HDO (0.1 M) using 1 M NaOH at 70 °C under 10 bar of oxygen yielded 97% sodium adipate after 4 h in the presence of a 1 wt% Au/C catalyst.[34] Au-Based materials present a variety of advantages over other noble metals, including high catalytic activity and stability which enable a higher selectivity to be obtained in selective oxidation processes of organic compounds in water compared with Pt- and Pd-based catalysts. These advantages appear because Au exhibits much better resistance to molecular $O_2$ and water.[35,36]

Furthermore, a number of previous research studies demonstrated that alloying Pd or Pt with Au enhanced significantly the catalytic activity and stability.[36–41] Supported bimetallic catalysts (2wt% Au–0.1wt% Pd and 2wt% Au–0.1wt% Pt) were reported to oxidize the aqueous solution of 1,6-HDO (0.1 M) to AA with yields up to 99% under 6 bar of oxygen and 34 bar of nitrogen at 140–160 °C for 2 h.[42] An Au–Pt/$ZrO_2$ catalyst ($n$Au/$n$Pt = 1 prepared by the co-wet impregnation method) was investigated in the aqueous phase oxidation of HDO (2.77 g HDO + 150 mL $H_2O$). After 48 h at 70 °C under 40 bar of air, full conversion of HDO was achieved with a maximum yield of AA of *ca.* 96%.[43,44] They hypothesized that the reaction pathway of HDO went through sequential oxidation (Scheme 1): first, HDO is oxidized to an intermediate 6-hydroxyhexanal (HH) which is a structural isomer of ε-caprolactol; the intermediate is subsequently oxidized to 6-hydroxyhexanoic acid (HA) which is a structural isomer of ε-caprolactone. Finally, AA was obtained by subsequent oxidation of HA *via* 6-oxohexanoic acid (OH).

The objective of this paper is to study the effect of different metal oxide supports for base-free HDO oxidation. We thus devoted our efforts to the development of an environmentally friendly process based on a base-free oxidation reaction using heterogeneous catalysts. Generally, reactions performed with base-free conditions (MgO) suffer from the leaching of $Mg^{2+}$.[45] Herein, we develop a new Au-based catalyst supported on $MgF_2$–MgO mixed solid phases, in which the catalytic performances are compared with those of various catalysts supported on different metal oxides.

## Results and discussion

The XRD patterns of the calcined samples at 500 °C are shown in Fig. 1. They confirmed the presence of crystallized

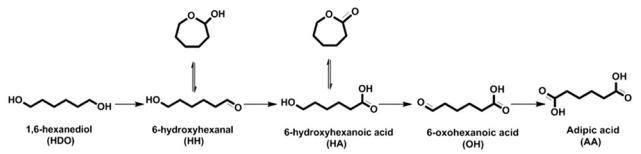


**Scheme 1** Oxidation of 1,6-hexanediol to adipic acid.

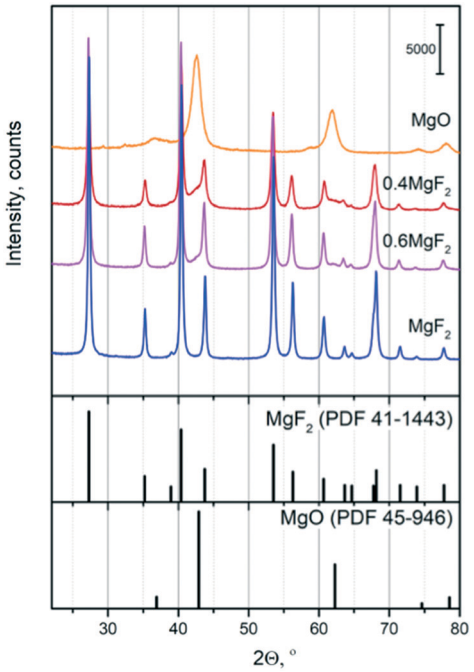


**Fig. 1** XRD patterns of the MgO, $MgF_2$ and $MgF_2$–MgO supports after calcination at 500 °C (top). $MgF_2$ and MgO PDF patterns (bottom).

$MgF_2$ and MgO phases. After calcination at 500 °C, $MgF_2$ and MgO phases were identified in the studied supports. Magnesium fluoride after calcination at 500 °C shows a typical $MgF_2$ X-ray diffraction pattern (Sellait, PDF 41-1443) and has a tetragonal structure ($P4_2/mnm$). No other diffraction peaks are detected showing the high purity of the phase. According to the JCPDS card (JCPDS card, No. 45-0946), the phase of the powders obtained from the magnesium precursor can be indexed to a cubic MgO structure ($Fm\bar{3}m$, periclase, PDF 45-496), which is consistent with the results reported in the literature.[50,51] Furthermore, it is worth nothing that the XRD patterns of the Au-based catalysts (not shown here) exhibited no diffraction peaks other than those associated with the supports suggesting that a small particle size of Au is achieved after sol immobilization.

To determine the effect of MgO in $MgF_2$–MgO mixed solid samples on the nature of the basic sites, temperature

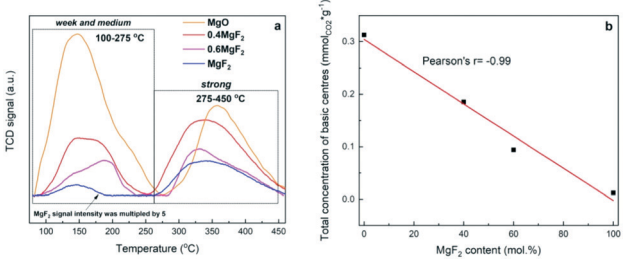


**Fig. 2** a) TPD-$CO_2$ profiles of $MgF_2$–MgO, MgO and $MgF_2$ supports; b) concentration of basic centres as a function of $MgF_2$ content in the sample.

programmed desorption of $CO_2$ (TPD-$CO_2$) was performed – Fig. 2.

The curves recorded (Fig. 2a) for the mixed systems $MgF_2$–MgO and those for pure $MgF_2$ and MgO reveal different types of desorption signals, indicating the presence of basic sites of different natures and strengths:[52] i) weak sites – desorption signals below 150 °C – correspond to weak sites assigned to $CO_2$ linearly bound to $OH^-$ or correspond to bicarbonate adsorbed at weakly basic OH groups; ii) medium strong sites – desorption signals in the range 150–350 °C – are assigned to $CO_2$ bridged with a magnesium cation and an oxygen anion; iii) strong sites – desorption signals above 350 °C – correspond to strong sites assigned to $CO_2$ linearly bound to $O^{2-}$. As reported by Aramendia *et al.*,[52] the basic sites correspond to three desorption temperature ranges, *viz.* 100–145 °C (weak sites), 170–225 °C (medium sites) and 240–345 °C (strong sites). The desorption peak appearing at the lowest temperature corresponds to bicarbonate adsorbed at weakly basic OH groups. The bidentate carbonate adsorbed at Mg–O pairs shows the desorption peak in the intermediate temperature range. Finally, the peak at the highest temperature corresponds to the unidentate carbonate bound to strongly basic $O^{2-}$ sites. According to ref. 52, the shape of the TPD-$CO_2$ profiles (Fig. 2a) clearly indicates the presence of weak and medium basic sites, which are responsible for the desorption peaks at about 100–275 °C, and strong sites from which $CO_2$ is desorbed at 275–450 °C.

For pure magnesium fluoride, two desorption peaks (at 144 and 334 °C) were recorded, which indicates the presence of a small number of weak and strong basic sites. It is known from our earlier results[53] that the surface area of $MgF_2$ contains weak acidic Lewis sites (coordinatively unsaturated magnesium ions) and basic sites (OH groups). The surface of MgO contains predominantly basic centres with the maximum of $CO_2$ desorption at 144 (weak sites) and 358 °C (strong sites), respectively. As reported by Wang *et al.*, on the basis of $CO_2$ adsorption measurements,[54] it has been shown that the basic centres on the surface of MgO are of two types (probably $O^{2-}$ ions and $OH^-$ groups). As reported by Prescott *et al.*,[55] the introduction of fluorine to MgO reduces the basic strength of $O^{2-}$ ($OH^-$). Also, Wuttke *et al.* reported that by increasing the fluorine content of magnesium oxide fluoride, the Lewis acidity increases whereas the basicity decreases.[56] This is clearly visible in the case of our systems, with increasing $MgF_2$ content, the total concentration of basic centers decreases in the sample – Fig. 2b and Table 1. The ratio of strong to weak and medium basic centers also changes. With the increase of $MgF_2$ in the support, the proportion of strong basic centers increases – Table 1.

The BET surface area decreased as the content of MgO in the $MgF_2$–MgO material decreased. The lowest average pore diameter was recorded for the bare MgO support with the highest surface area (Table 2).

The TEM images of the Au-based catalysts are shown in Fig. 3. For each sample, approximately 300 particles were used to estimate the average particle size. The average particle size of PVA-stabilized Au NPs was 3 nm (not shown). The average particle sizes of Au nanoparticles were conserved after immobilization on different supports (Fig. 3). Indeed, the Au NPs deposited on the supports were monodispersed with an average size of 3.6 nm ± 0.8 nm and no significant agglomeration of gold nanoparticles was detected.

As mentioned in the introduction, several works have shown that the heterogeneous catalysts based on noble metals were efficient for catalytic oxidation. The effect of noble metals on HDO conversion and product selectivity is presented in Table 3. The carbon balance was always over *ca.* 90%. The non-complete carbon balance can be attributed to the adsorption of the intermediate aldehyde (HA), or the formation of gaseous products by decarbonylation of aldehydes, decarboxylation of acid or di-acid products, or over oxidation.[43,44]

At 100 °C under 6 bar of $O_2$, and for the same reaction time, Au NPs showed a higher catalytic activity (58%) toward HDO conversion compared to Pd NPs (27%). Whatever the noble metal, the main product of the reaction was the intermediate HA ($S_{HA}$ = 58%). This result suggests that both catalysts preferentially oxidize HDO and the HA desorption is the rate-determining step of the reaction. Moreover, AA formation was favored in the presence of the Au/MgO catalyst with a selectivity of 23%. For that reason, Au-based catalysts were chosen in the selective oxidation of HDO. Au/MgO, Au/BaO, Au/NiO and Au/$TiO_2$ catalysts were investigated in the catalytic oxidation of HDO. The effect of the support on the catalytic activity and selectivity to reaction products is presented in Table 4. First, it is worth mentioning that the carbon balance at the defined conversions was always higher than 90%. Au/MgO showed a higher catalytic activity ($X_{HDO}$ = 58%) compared to the other Au-supported catalysts in the present work with 23% selectivity to AA. At 100 °C under 6 bar of $O_2$, and for 3 h reaction time, the catalytic activity for HDO conversion and selectivity to AA followed the order:

**Table 1** $CO_2$-TPD results for $MgF_2$–MgO, MgO and $MgF_2$ supports

| Sample | Ratio of peak surfaces[a] | Number of basic sites, $mmol_{CO_2}\ g^{-1}$ | | |
|---|---|---|---|---|
| | | Total | 100–275 °C, weak and medium | 275–450 °C, strong |
| MgO | 0.5 | 0.3126 | 0.2074 | 0.1052 |
| 0.4$MgF_2$ | 1.8 | 0.1854 | 0.0663 | 0.1191 |
| 0.6$MgF_2$ | 1.7 | 0.0940 | 0.0350 | 0.0590 |
| $MgF_2$ | 7.4 | 0.0120 | 0.0014 | 0.0106 |

[a] Ratio of the peak area at 275–450 °C to the peak area at 100–275 °C.

**Table 2** Specific surface area, total pore volume and average pore diameter as determined from the BET and BJH methods

| Sample | BET surface area, $m^2\ g^{-1}$ | Total pore volume, $cm^3\ g^{-1}$ | Average pore diameter, nm |
|---|---|---|---|
| MgO | 100 | 0.2 | 5.5 |
| $0.4MgF_2$ | 81 | 0.4 | 16.8 |
| $0.6MgF_2$ | 51 | 0.3 | 23.8 |
| $MgF_2$ | 29 | 0.2 | 22.4 |

MgO > BaO > NiO > $TiO_2$, which indicates that the active sites of the support play an important role in the oxidation reactions.[57] Indeed, this was in agreement with Davis *et al.*[58] They said that the number of hydroxyl groups on the surface of the catalyst will increase by using basic supports which thus trigger the oxidation of HDO.

The basic oxide support (MgO) reacts with water to form a weak base inorganic compound ($Mg(OH)_2$) resulting in the increase of pH of the reaction mixture.[45] In contrast, the pH of the acidic mixture will not change in the presence of much less basic $TiO_2$.[59] This result is in good agreement with the report of Ebitani *et al.*, who investigated the oxidation of 5-hydroxymethylfurfural into 2,5-furandicarboxylic acid. They reported that catalysts using neutral or acidic supports exhibited a lower catalytic activity than those with basic supports [$SiO_2$ < activated carbon (AC) < $Al_2O_3$ < MgO < hydrotalcite (HT)].[60] Although the catalytic activity depends on the basic sites on the surface of the catalyst, by using basic oxides (NiO, BaO, MgO), hydroxide ions in aqueous solutions will be formed, dissolving part of the support. The leaching of $Mg^{2+}$ from HT was detected during the oxidation of HMF in the presence of a Au/HT catalyst.[61] The pH values obtained before ($pH_{initial}$ = 7.6) and after catalytic tests ($pH_{final}$ = 9.4, Table 4) and ICP-OES measurements (110 ppm for Au/MgO) confirmed the dissolution of the supports; according to the literature,[59] the acid formed during the reaction lowered the pH of the reaction medium, due to the acid–base reaction. Then, the formation of acidic products (AA and HA) will intensify the support dissolution resulting in lower pH values at the end of the reaction. This means that the catalysts with basic supports are very active, but they are not stable, due to the leaching of the support. Only the solution corresponding to the $Au/TiO_2$ catalyst showed an acidic pH value with negligible leaching (15 ppm). Finally, whatever the support, HA was the main product formed. The highest selectivity ($S_{HA}$ = 60%) was recorded in the presence of Au/BaO.

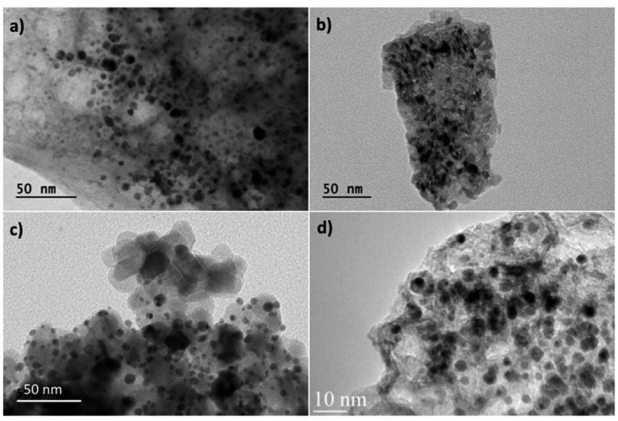


**Fig. 3** TEM images of the (a) Au/MgO, (b) Au/NiO, (c) $Au/TiO_2$ and (d) supported $Au/0.6MgF_2$–0.4MgO catalysts.

**Table 3** Conversion and selectivity to products during oxidation of HDO. Reaction conditions: HDO 14 mmol $L^{-1}$, 20 mL $H_2O$, 100 °C, 6 bar $O_2$, 600 rpm, 3 h, $n_{HDO}/n_M$ = 100. HDO: 1,6-hexanediol, M; Au or Pd

| Catalyst | $X_{HDO}$ (%) | $S_{HA}$ (%) | $S_{AA}$ (%) | CB (%) |
|---|---|---|---|---|
| Au/MgO | 58 | 58 | 23 | 90 |
| Pd/MgO | 27 | 58 | 15 | 93 |

Unfortunately, during the catalytic tests, leaching issues at the end of the reaction have been noted. Nevertheless, apparently the basic properties of the supports contribute significantly to the catalytic activity of the final materials. Their catalytic performances strongly depend on the basicity of the support. For that reason, the basicity effect was studied by changing the amount of MgO and $MgF_2$ in MgO–$MgF_2$ mixed phases. The effect of MgO addition to $Au/MgF_2$ catalysts on conversion and selectivity to reaction products is shown in Fig. 4.

First, it should be noted that the carbon balance at the defined conversions was always close to 90%. $Au/MgF_2$ exhibited low catalytic activity, similar to the $Au/TiO_2$ catalyst (11% HDO conversion) with negligible formation of AA ($S_{AA}$ = 1%). Over the $Au/MgF_2$ catalyst, there was no change in the pH value at the beginning and end of the reaction suggesting the absence of leaching. Therefore, the lower catalytic performance can be assigned to the acidic reaction medium which does not favor the Au-based solid catalytic functions. Increasing the content of MgO to an certain level in the mixed phase support (MgO–$MgF_2$) enhanced the catalytic performance (Fig. 5 and 2b).

The $X_{HDO}$ and $S_{AA}$ increased from 11 and 1% to 62 and 33%, respectively, when the content of MgO was increased from 0 to 60%. Surprisingly, $Au/0.4MgF_2$–0.6MgO and Au/MgO showed similar catalytic activities (62% and 59%, respectively). However, the effect was mainly on the AA selectivity (33% *vs.* 23%, Fig. 4). These corroborate the synergic effect between $MgF_2$ and MgO for the activity and

**Table 4** Effect of the support for gold nanoparticles on conversion and selectivity to reaction products during catalytic oxidation of HDO. Reaction conditions: HDO 14 mmol $L^{-1}$, 20 mL $H_2O$, 100 °C, 6 bar $O_2$, 600 rpm, 3 h, $n_{HDO}/n_{Au}$ = 100, $pH_{initial}$ = 7.6. HDO: 1,6-hexanediol

| Catalyst | $X_{HDO}$ (%) | $S_{HA}$ (%) | $S_{AA}$ (%) | CB (%) | $pH_{final}$ |
|---|---|---|---|---|---|
| $Au/TiO_2$ | 16 | 26 | 5 | 90 | 5.0 |
| Au/NiO | 23 | 39 | 6 | 91 | 5.9 |
| Au/BaO | 35 | 60 | 15 | 91 | 8.2 |
| Au/MgO | 58 | 58 | 23 | 90 | 9.4 |
| $Au/0.6MgF_2$–0.4MgO | 42 | 41 | 33 | 89 | 5.6 |

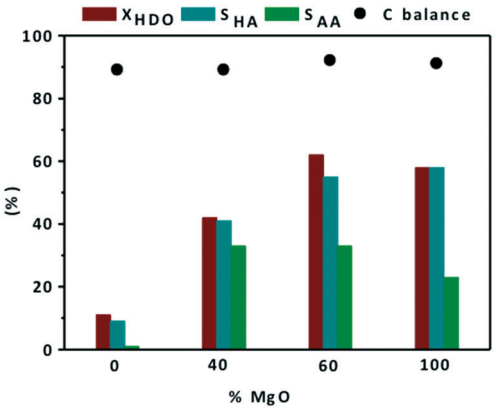


Fig. 4 Effect of MgO addition to Au/$MgF_2$ catalysts on conversion and selectivity to reaction products during catalytic oxidation of HDO. Reaction conditions: HDO 14 mmol $L^{-1}$, 20 mL $H_2O$, 100 °C, 6 bar $O_2$, 600 rpm, 3 h, $n_{HDO}/n_{Au}$ = 100. (■) Conversion of 1,6-hexandiol, (■) selectivity to 6-hydroxyhexanoic acid, (■) selectivity to adipic acid, and (●) carbon balance.

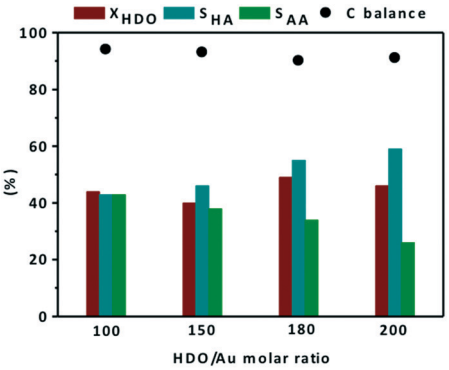


Fig. 6 Effect of the HDO/Au molar ratio on conversion and selectivity to reaction products during catalytic oxidation of HDO. Reaction conditions: 2 mL aqueous solution of HDO (14 mmol $L^{-1}$), 110 °C, 15 bar of air, 600 rpm, 4 h, 10 mg Au/0.6$MgF_2$–0.4MgO. (■) conversion of 1,6-hexandiol, (■) selectivity to 6-hydroxyhexanoic acid, (■) selectivity to adipic acid, and (●) carbon balance.

selectivity to AA. These data are consistent with observations during catalytic oxidation of furfural to furoic acid at 110 °C, under 26 bar of $O_2$, for 2 h over the Au/$MgF_2$–MgO catalyst; they showed that upon increasing the MgO content from 0 to 60%, the conversion of furfural and yield of furoic acid increased from 20 and 5% to 95 and 99%, respectively. Under the same conditions, they also found that 60 mol% of MgO in the mixed phase material ($MgF_2$–MgO) was already enough to provide the same catalytic activity as that of pure MgO.[47,57] At the end, ICP-OES measurements showed much lower Mg leaching (82 ppm) in the case of mixed phases than in the case of MgO (110 ppm). This confirms that the leaching of Mg in the mixture of $MgF_2$ and MgO was limited by diluting the basic sites in the support.

The effect of the HDO/Au ratio was studied using a screening pressure reactor (SPR) at 110 °C under 15 bar of air for 4 h in the presence of the Au/0.6$MgF_2$–0.4MgO catalyst. The effect of the HDO/Au ratio on catalytic conversion and product selectivity is shown in Fig. 6. In these experiments, the total volume of water was fixed and the number of moles of HDO was adjusted by varying the amount of HDO added.

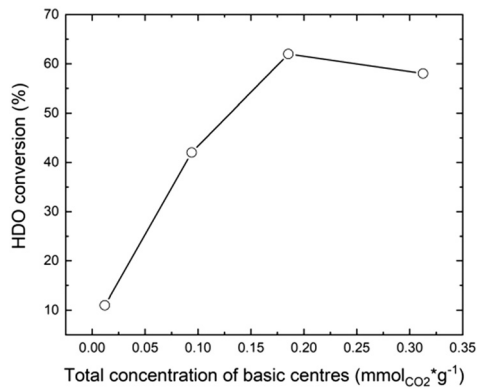


Fig. 5 HDO conversion as a function of strong basic site quantity.

At 110 °C and under 15 bar of air, whatever the HDO/Au molar ratio, the catalytic conversion of HDO remained roughly constant (40–49%). Under these conditions, the selectivity to the monoacid compound (HA) resulting from the first oxidation of HDO increased from 43 to 59%, whereas the selectivity to the diacid compound (AA) decreased from 43 to 26%, as the HDO/Au molar ratio increased from 100 to 200. This tendency agrees with the literature dealing with the selective oxidation of 5-hydromethylfurfural (HMF) to 2,5-furandicarboxylic (FDCA) at 110 °C under 26 bar of air over an Au/MgO catalyst.[47,57] In this study, they reported that the yield of the intermediate monacids [5-hydroxymethyl-2-furancarboxylic monoacid (HMFCA) and 5-formyl-2-furancaboxylic acid (FFCA)] increased from 5 to 70%, whereas the selectivity to diacid molecules [2,5-furandicarboxylic (FDCA)] decreased from 95 to 30% as the HMF/Au molar ratio increased from 100 to 400. It is worth mentioning that the highest selectivity to adipic acid (43%) at 49% conversion over the monometallic catalyst (Au/0.6$MgF_2$–0.4MgO) is comparable with the literature when using the bimetallic Au–Pt/$ZrO_2$ catalyst under similar reaction conditions (40% selectivity at 50% conversion).[43] Finally, the mass balance in the range of HDO/Au molar ratios was >90%.

# Experimental

### Supports

NiO, MgO, and $TiO_2$ were purchased from Sigma Aldrich®. The reaction between $4MgCO_3{\cdot}Mg(OH)_2{\cdot}5H_2O$ powder (POCH – Polish Chemicals Reagents) and controlled amounts of a 40 wt% aqueous solution of HF (POCH – Polish Chemicals Reagents) formed the supports ($MgF_2$ and $MgF_2$–MgO) with different $MgF_2$/MgO ratios.[46,47] 40, 60 and 100 mol% of $MgF_2$ in the support were obtained by modifying the amount of HF. The resulting dense gels of $MgF_2$-unreacted magnesium carbonate were subjected to ageing for 40 h at room temperature then dried at 80 °C for 24 h before being

calcined under air flow (50 mL $min^{-1}$) at 500 °C for 4 h. The $MgF_2$–MgO samples were labeled as $0.4MgF_2$–0.6MgO and $0.6MgF_2$–0.4MgO. BaO was obtained by calcination of 1 g of $BaNO_3$ (Sigma-Aldrich) at 600 °C for 6 h (20 °C $min^{-1}$).

### Catalyst preparation

The supported Au catalysts were prepared by using the sol-immobilization method.[48,49] 2 wt% polyvinyl alcohol solution (PVA, Sigma-Aldrich, MW 55 000 g $mol^{-1}$) was dropped to the $HAuCl_4$ (99.9%, Sigma-Aldrich) water solution (0.5 mM) under magnetic stirring [PVA/Au (w/w) = 1.2]. To reduce the gold particles, a solution of $NaBH_4$ (98%, Sigma-Aldrich, 0.1 M, $NaBH_4$/Au (mol/mol) = 5] was added to the PVA/Au solution. A light-red color was obtained indicating the reduction of gold. After 30 minutes of sol generation, the Au nanoparticles were immobilized by adding different supports ($TiO_2$, NiO, BaO, MgO, $0.4MgF_2$–0.6MgO and $0.6MgF_2$–0.4MgO) under vigorous stirring. Then, the solid was filtered and washed with ethanol and hot water. Finally, the catalyst was dried at 100 °C for 1 h. The final loading of gold was ~2 wt% for all the Au-containing samples, as determined by ICP analysis.

### Characterization of catalysts

The powder X-ray diffraction patterns (XRD) of the samples were recorded using a Bruker AXS D8 Advance diffractometer equipped with a nickel filter, a copper tube ($\lambda K\alpha$ (Cu) = 1.54184 Å) and a multi-channel fast detector. The samples were scanned at 0.014° $s^{-1}$ over the range $20 \leq 2\theta \leq 80°$. The XRD data for the well-crystallized phases of $MgF_2$ and MgO calcined at 900 °C for 4 h were used to determine the composition of the $MgF_2$–MgO supports. Then, the content of MgO and $MgF_2$ could be determined by comparing the intensities of the diffraction peaks of the studied samples with those of the mixture of $MgF_2$ and MgO calcined at 900 °C, containing 85, 70 or 30 mol% of $MgF_2$. The DQuant program was used for the calculations, taking into consideration the XRD patterns of MgO and $MgF_2$ which exhibited diffraction peaks at $2\theta$ = 36.92°, 42.92°, and 62.29° (MgO) and at $2\theta$ = 35.21°, 53.48° and 60.60° ($MgF_2$).[50] The (BET) specific surface areas of the catalysts were determined by $N_2$ adsorption at −196 °C using a Micromeritics ASAP 2010 sorptometer. The Barrett–Joyner–Halenda (BJH) method was used to determine the total pore volume and average pore radius. TEM images were obtained by using an FEI Tecnai microscope. A drop of the particles dispersed in ethanol was placed on a carbon-coated copper-grid. Elemental analysis of the Au-based catalysts was carried out by ICP-OES (inductively coupled plasma optical emission spectrometry) analysis by using Agilent 720-ES ICP-OES equipment combined with a Vulcan 42S automated digestion system. The pH value was measured for each sample using a pH meter (FE20 FiveEasy). TPD-$CO_2$ was performed on a Micromeritics ChemiSorb 2705. Prior to $CO_2$ adsorption, the samples were pre-treated *in situ* in He at 480 °C for 30 min to remove the molecules adsorbed on the surface. Carbon dioxide was adsorbed at 50 °C for 1 h. TPD-$CO_2$ analysis was carried out in the temperature range of 50–480 °C using a ramp rate of 10 °C $min^{-1}$. The desorption of $CO_2$ was monitored with a thermal conductivity detector (TCD) and the signal intensity was normalized to 1 g for each sample studied.

### HDO oxidation catalytic tests

The catalytic oxidations of HDO were carried out using two catalytic systems: first, the reactions were carried out in a 30 mL TOPIndustry autoclave reactor equipped with a high precision heating system and a mechanical stirrer. In a typical experiment, an aqueous solution (20 mL) of HDO and the appropriate amount of catalyst that corresponds to the HDO/metal molar ratio of 100 were introduced into the reactor. After this, the reactor was closed and purged with a flow of oxygen. The reaction was carried out under 6 bar of $O_2$, at 100 °C, 600 rpm for 3 h. The time necessary to reach the desired temperature was not considered in the reaction time; indeed the 3 hours of reaction started just when the system reached the right temperature. The second system is a multi-reactor system: the screening pressure reactor (SPR). It consists of 24 parallel batch reactors with a final volume of 6 mL, in which each reactor was loaded with an aqueous HDO solution (2 mL, 14 mmol $L^{-1}$) and the considered Au-based catalyst (*ca.* 10 mg). The reaction was carried out under 15 bar of air, at 110 °C, 600 rpm for 4 h. At the end of the reactions, the autoclave was cooled, the pressure was released, and the suspension was collected and filtered with a nylon membrane filter (0.2 μm). AA, HDO, and HA were analyzed using a high performance liquid chromatograph (HPLC, Waters 2410 RJ) equipped with refractive index (RI) and UV detectors and a Rezex ROA–organic acid $H^+$ column (∅ 7.8 mm × 300 mm). Dilute $H_2SO_4$ (5 mM, 0.5 mL $min^{-1}$) was used as a mobile phase. The response factor was determined experimentally for the commercial compounds. It was therefore possible to calculate conversion ($X$), selectivity ($S$) and carbon balance (CB), according to the following formulas:

$$X_{\mathrm{HDO}}\,(\%) = \frac{n_{\mathrm{HDO}_0} - n_{\mathrm{HDO}_f}}{n_{\mathrm{HDO}_0}} \times 100$$

$$S_{\mathrm{product}}\,(\%) = \frac{n_{\mathrm{product}_f}}{n_{\mathrm{HDO}_0} - n_{\mathrm{HDO}_f}} \times 100$$

$$\text{Carbon balance}(\mathrm{CB}) = \frac{n_{\mathrm{HDO}_f} + n_{\mathrm{AA}_f} + n_{\mathrm{HA}_f}}{n_{\mathrm{HDO}_0}} \times 100$$

where $n_{\mathrm{HDO}_i}$ is the initial number of moles of HDO, $n_{\mathrm{HDO}_f}$ is the final number of moles of HDO, $n_{\mathrm{product}_f}$ is the final number of moles of products, $n_{\mathrm{AA}_f}$ is the final number of moles of adipic acid, and $n_{\mathrm{HA}_f}$ is the final number of moles of HA.

## Conclusions

The selective aqueous phase oxidation of 1,6-hexanediol to adipic acid was investigated under base-free conditions in the presence of Au-basic oxide materials. The formation of AA followed multiple sequential oxidations of HDO *via* the aldehyde. The catalytic performance of Au-based catalysts prepared by the sol immobilization method showed that the conversions and selectivity to AA highly depend on the basicity of the support. Au/MgO was the most efficient catalyst among the other base oxides. However, the main drawback was the leaching of Mg. Subsequently, new Au/$MgF_2$–MgO-based catalysts were developed in which the active MgO phase was diluted within an inactive $MgF_2$ phase. This development limited the leaching of Mg. The highest selectivity to adipic acid (43%) was achieved at 110 °C under 15 bar of air in the presence of 2 wt% Au/0.6$MgF_2$–0.4MgO with 100 as the HDO/Au molar ratio.

## Conflicts of interest

There are no conflicts to declare.

## Acknowledgements

The REALCAT platform benefits from a state subsidy administrated by the French National Research Agency (ANR) within the frame of the 'Investments for the Future' program (PIA), with the contractual reference 'ANR-11-EQPX-0037'. The European Union, through the FEDER funding administered by the Hauts-de-France Region, has co-financed the platform. Centrale Lille, CNRS, and the University of Lille as well as the Centrale Initiatives Foundation are thanked for their financial contributions to the acquisition and implementation of the equipment of the REALCAT platform. Chevreul Institute (FR 2638), Ministère de l'Enseignement Supérieur, de la Recherche et de l'Innovation, Hauts-de-France Region and FEDER are acknowledged for supporting and partially funding this work.

## Notes and references

1 J. P. Oppenheim and G. L. Dickerson, *Kirk-Othmer Encycl. Chem. Technol.*, 2000, 553–582.
2 S. Van de Vyver and Y. Román-Leshkov, *Catal. Sci. Technol.*, 2013, **3**, 1465–1479.
3 R. Beerthuis, G. Rothenberg and N. Raveendran Shiju, *Green Chem.*, 2015, **17**, 1341–1361.
4 A. Mazzi, S. Paul, F. Cavani and R. Wojcieszak, *ChemCatChem*, 2018, **10**, 3680–3682.
5 A. Rahman, M. Mupa and C. Mahamadi, *Catal. Lett.*, 2016, **146**, 788–799.
6 L.-X. Xu, C.-H. He, M.-Q. Zhu and S. Fang, *Catal. Lett.*, 2007, **114**, 202–205.
7 B. P. C. Hereijgers and B. M. Weckhuysen, *J. Catal.*, 2010, **270**, 16–25.
8 A. Dutta, M. Pramanik, A. K. Patra, M. Nandi, H. Uyama and A. Bhaumik, *Chem. Commun.*, 2012, **48**, 6738–6740.
9 M. Moudjahed, L. Dermeche, S. Benadji, T. Mazari and C. Rabia, *J. Mol. Catal. A: Chem.*, 2016, **414**, 72–77.
10 K. Sato, M. Aoki and R. Noyori, *Science*, 1998, **281**, 1646–1647.
11 S.-O. Lee, R. Raja, K. D. M. Harris, J. M. Thomas, B. F. G. Johnson and G. Sankar, *Angew. Chem., Int. Ed.*, 2003, **42**, 1520–1523.
12 F. Cavani, G. Centi, S. Perathoner and F. Trifirò, *Sustainable Industrial Processes*, Wiley-VCH, Weinheim, 2007.
13 M. Röper, in *Stud. Surf. Sci. Catal.*, Elsevier, 1991, pp. 381–429.
14 J. Han, *Energy Convers. Manage.*, 2016, **129**, 75–80.
15 S. Gunukula and R. P. Anex, *Biofuels, Bioprod. Biorefin.*, 2017, **11**, 897–907.
16 T. R. Boussie, E. L. Dias, Z. M. Fresco and V. J. Murphy, Production of Adipic Acid and Derivatives from Carbohydrate-Containing Materials, *US Pat.*, 2010/0317822 to Rennovia, 2010.
17 G. M. Diamond, V. Murphy and T. R. Boussie, *Mod. Appl. High Throughput RD Heterog. Catal.*, ed. A. Hagemeyer and F. Volpe, Bentham Sci. Publ., 2014, pp. 288–309.
18 T. R. Boussie, E. L. Dias, Z. M. Fresco, V. J. Murphy, J. Shoemaker, R. Archer and H. Jiang, Production of Adipic Acid and Derivatives from Carbohydrate-Containing Materials, *US Pat.*, 2014/8669397 to Rennovia, 2014.
19 J. Q. Bond, D. M. Alonso, R. M. West and J. A. Dumesic, *Langmuir*, 2010, **26**, 16291–16298.
20 (*a*) S. Solmi, E. Rozhko, A. Malmusi, T. Tabanelli, S. Albonetti, F. Basile, S. Agnoli and F. Cavani, *Appl. Catal., A*, 2018, **557**, 89–98; (*b*) E. Amadio, J. Gonzalez-Fabra, D. Carraro, W. Denis, B. Gjoka, C. Zonta, K. Bartik, F. Cavani, S. Solmi, C. Bo and G. Licini, *Adv. Synth. Catal.*, 2018, **360**, 3286–3296.
21 T. Buntara, S. Noel, P. H. Phua, I. Melián-Cabrera, J. G. de Vries and H. J. Heeres, *Top. Catal.*, 2012, **55**, 612–619.
22 T. Buntara, S. Noel, P. H. Phua, I. Melián-Cabrera, J. G. de Vries and H. J. Heeres, *Angew. Chem., Int. Ed.*, 2011, **50**, 7083–7087.
23 K. Chen, S. Koso, T. Kubota, Y. Nakagawa and K. Tomishige, *ChemCatChem*, 2010, **2**, 547–555.
24 M. Chia, Y. J. Pagán-Torres, D. Hibbitts, Q. Tan, H. N. Pham, A. K. Datye, M. Neurock, R. J. Davis and J. A. Dumesic, *J. Am. Chem. Soc.*, 2011, **133**, 12675–12689.
25 S. P. Burt, K. J. Barnett, D. J. McClelland, P. Wolf, J. A. Dumesic, G. W. Huber and I. Hermans, *Green Chem.*, 2017, **19**, 1390–1398.
26 A. Said, D. Da Silva Perez, N. Perret, C. Pinel and M. Besson, *ChemCatChem*, 2017, **9**, 2768–2783.
27 A. Corma, S. Iborra and A. Velty, *Chem. Rev.*, 2007, **107**, 2411–2502.
28 S. H. Krishna, D. J. McClelland, Q. A. Rashke, J. A. Dumesic and G. W. Huber, *Green Chem.*, 2017, **19**, 1278–1285.
29 M. Faber, Process for Producing Adipic Acid from Biomass, *US Pat.*, 1983/4400468 to Hydrocarbon Research, 1983.
30 J. Xie, B. Huang, K. Yin, H. N. Pham, R. R. Unocic, A. K. Datye and R. J. Davis, *ACS Catal.*, 2016, **6**, 4206–4217.

31 M. S. Ide, D. D. Falcone and R. J. Davis, *J. Catal.*, 2014, **311**, 295–305.
32 M. S. Ide and R. J. Davis, *J. Catal.*, 2013, **308**, 50–59.
33 S. E. Davis, M. S. Ide and R. J. Davis, *Green Chem.*, 2013, **15**, 17–45.
34 T. Wang, M. S. Ide, M. R. Nolan, R. J. Davis and B. H. Shanks, *Energy Environ. Focus*, 2016, **5**, 13–17.
35 X. Wan, C. Zhou, J. Chen, W. Deng, Q. Zhang, Y. Yang and Y. Wang, *ACS Catal.*, 2014, **4**, 2175–2185.
36 (*a*) A. Lolli, S. Albonetti, L. Utili, R. Amadori, F. Ospitali, C. Lucarelli and F. Cavani, *Appl. Catal., A*, 2015, **504**, 408–419; (*b*) S. Solmi, C. Morreale, F. Ospitali, S. Agnoli and F. Cavani, *ChemCatChem*, 2017, **9**, 2797–2806.
37 C. L. Bianchi, P. Canton, N. Dimitratos, F. Porta and L. Prati, *Catal. Today*, 2005, **102–103**, 203–212.
38 D. I. Enache, J. K. Edwards, P. Landon, B. Solsona-Espriu, A. F. Carley, A. A. Herzing, M. Watanabe, C. J. Kiely, D. W. Knight and G. J. Hutchings, *Science*, 2006, **311**, 362–365.
39 A. Villa, D. Wang, D. Su, G. M. Veith and L. Prati, *Phys. Chem. Chem. Phys.*, 2010, **12**, 2183–2189.
40 W. Hou, N. Dehm and R. Scott, *J. Catal.*, 2008, **253**, 22–27.
41 N. Dimitratos, J. A. Lopez-Sanchez and G. J. Hutchings, *Chem. Sci.*, 2012, **3**, 20–44.
42 E. L. Dias, V. J. Murphy and J. A. W. Shoemaker, Process for Production of Adipic Acid from 1,6-Hexanediol, *US Pat.*, 2013/0331606 to Rennovia, 2015.
43 M. Mounguengui-Diallo, F. Vermersch, N. Perret, C. Pinel and M. Besson, *Appl. Catal., A*, 2018, **551**, 88–97.
44 M. Mounguengui-Diallo, A. Sadier, D. Da Silva Perez, C. Nikitine, L. Puchot, Y. Habibi, C. Pinel, N. Perret and M. Besson, *New J. Chem.*, 2019, **43**, 9873–9885.
45 M. Douthwaite, X. Huang, S. Iqbal, P. J. Miedziak, G. L. Brett, S. A. Kondrat, J. K. Edwards, M. Sankar, D. W. Knight, D. Bethell and G. Hutchings, *Catal. Sci. Technol.*, 2017, **7**, 5284–5293.
46 M. Zieliński, A. Kiderys, M. Pietrowski, I. Tomska-Foralewska and M. Wojciechowska, *Catal. Commun.*, 2016, **76**, 54–57.
47 M. Zieliński, *Appl. Catal., A*, 2012, **449**, 15–22.
48 C. Ferraz, M. Zielinski, M. Pietrowski, S. Heyte, F. Dumeignil, L. Marcia Rossi and R. Wojcieszak, *ACS Sustainable Chem. Eng.*, 2018, **6**, 16332–16340.
49 N. Dimitratos, J. A. Lopez-Sanchez, D. Morgan, A. Carley, L. Prati and G. J. Hutchings, *Catal. Today*, 2007, **122**, 317–324.
50 K. Chhor, J. F. Bocquet and C. Pommier, *Mater. Chem. Phys.*, 1995, **40**, 63–68.
51 E. Alvarado, L. M. Torres-Martinez, A. F. Fuentes and P. Quintana, *Polyhedron*, 2000, **19**, 2345–2351.
52 (*a*) Z. Liu, J. A. Cortés-Concepcion, M. Mustian and M. D. Amiridis, *Appl. Catal., A*, 2006, **302**, 232–236; (*b*) M. A. Aramendia, V. Borau, C. Jimenez, J. M. Marinas, J. R. Ruiz and F. J. Urbano, *Appl. Catal., A*, 2003, **244**, 207–215.
53 M. Wojciechowska, B. Czajka, M. Pietrowski and M. Zieliński, *Catal. Lett.*, 2000, **66**, 147–153.
54 J. A. Wang, O. Novaro and X. Bokhimi, *J. Phys. Chem. B*, 1997, **101**, 7448–7451.
55 H. A. Prescott, Z.-J. Li, E. Kemnitz, J. Deutsch and H. Lieske, *J. Mater. Chem.*, 2005, **15**, 4616–4628.
56 S. Wuttke, S. M. Coman, J. Kröhnert, F. C. Jentoft and E. Kemnitz, *Catal. Today*, 2010, **152**, 2–10.
57 C. P. Ferraz, M. A. S. Garcia, É. Teixeira-Neto and L. M. Rossi, *RSC Adv.*, 2016, **6**, 25279–25285.
58 B. N. Zope, D. D. Hibbitts, M. Neurock and R. J. Davis, *Science*, 2010, **330**, 70–74.
59 J. A. Duffy, *J. Chem. Educ.*, 1996, **73**, 1138–1142.
60 N. K. Gupta, S. Nishimura, A. Takagaki and K. Ebitani, *Green Chem.*, 2011, **13**, 824–827.
61 B. N. Zope, S. E. Davis and R. J. Davis, *Top. Catal.*, 2012, **55**, 24–32.

 